Experimental report for expt no. 28-01 1082

Studying the effect of confinement on inorganic nanowires

Dr Thomas Chamberlain, University of Leeds.

Summary:

The preparation of inorganic nanomaterials with a desired structure and specific properties requires the ability to strictly control their size, shape and composition. A series of chemical reactions with platinum compounds carried out within the 1.5 nm wide channel of single-walled carbon nanotubes (SWNTs) have demonstrated SWNTs as both a very effective reaction vessel and a template for the formation of nanocrystals of platinum di-iodide and platinum di-sulphide, materials that are difficult to synthesise in the form of nanoparticles by traditional synthetic methods. The stepwise synthesis inside nanotubes has enabled the formation of Pt compounds to be monitored at each step of the reaction by aberration corrected high resolution transmission electron microscopy (AC-HRTEM) imaging, verifying the atomic structures of the products, and by an innovative combination of fluorescence-detected X-ray absorption spectroscopy (FD-XAS) and Raman spectroscopy, monitoring of the oxidation states of the platinum guest-compounds within the nanotube and the vibrational properties of the host-SWNT respectively. This coupling of complementary spectroscopies reveals that electron transfer between the guest-compound and the host-SWNT can occur in either direction depending on the composition and structure of the latter. Despite the significant didactic value of the tepwise synthesis for understanding inorganic reactivity at the nanoscale, this approach has limited preparative potential because of the lack of stoichiometric control in the resultant inorganic nanomaterials. A new approach for nanoscale synthesis in nanotubes developed in this study utilises the versatile coordination chemistry of Pt which has enabled the insertion of the required chemical elements (e.g. metal and halogens or chalcogens) into the nanoreactor in the correct proportions for the formation of PtI_2 and PtS_2 with the correct stoichiometry and structure.

Introduction:

The development of new methodologies for the controlled arrangement of molecules and atoms into highly ordered arrays is vitally important for harnessing the functional properties emerging at the nanoscale due to the effects of quantum confinement, which are essential for catalysis, electronic and biomedical applications. The cylindrical internal cavity of SWNTs provides a powerful template for control of the exact positions and orientations of the molecules and atoms and has been successfully applied to the construction of nanoscale architectures from a variety of metals,[1-3] organic molecules,[4-6] and inorganic compounds[7-12] inserted within SWNTs. A striking example of the power of this

technique was reported by Chuvilin *et al.* who demonstrated that sulfur-terminated graphene nanoribbons, practically impossible to synthesise by synthetic chemistry routes, can be spontaneously formed from inexpensive, readily available precursors, such as tetrathiafulvalene, in one step within SWNTs.[13, 14] More recently, very narrow double-walled carbon nanotubes have been demonstrated as effective containers for templating the important, but still illusive, allotrope of carbon, carbyne.[15] Shi *et al.* demonstrated that at high temperature the host nanotube can template the formation of this new allotrope of carbon and protect it from undesired side reactions, thus paving the way for the first bulk production of carbyne. These examples clearly demonstrate the intrinsic ability of the SWNTs to direct chemical reactions and control the dimensionality of products formed inside nanotubes, where the product structure is crucially determined by the internal diameter of the nanotube.

Low-dimensional inorganic materials, including transition metal chalcogenides, are currently of particular interest due to the fact that their semiconducting electronic properties can be precisely tuned by shaping their structures into nanoribbons, in analogous fashion to graphene.[16] While the host-nanotube can control the dimensions of the inorganic structure, control of the stoichiometry is typically achieved by immersing open SWNTs into a molten inorganic compound with the desired, predetermined chemical composition, so that the nanotube becomes filled with cations and anions in the correct ratio due to capillary forces. A now ubiquitous technique, it has led to the encapsulation of many inorganic compounds, such as lanthanide halides,[17] potassium iodide,[18] cobalt iodide,[19] tin telluride,[20] and barium diiodide,[9] yielding nanostructures with well-defined composition and morphology, and physical properties often different to those found in the bulk. However, the need to melt inorganic compounds in this method imposes severe limitations on the choice of encapsulated materials, as many important inorganic materials, such as metal oxides, decompose before melting or melt at extremely high temperature, *e.g.* the melting point of MoS_2 is 1185 °C.

The direct synthesis of inorganic compounds inside nanotubes can offer an attractive alternative which may significantly broaden the scope of inorganic compounds that are confined at the nanoscale. The nanotube in this case acts simultaneously as a nanoscale reactor and a template for controlling the dimensions of inorganic structures. Inorganic synthesis inside nanotubes has been successfully applied by Eliseev *et al.* to the synthesis of CdS@SWNT by treating pre-encapsulated CdI_2, inserted into nanotubes from the molten phase, with sulfur at high temperature.[21] This elegantly avoids the problem that bulk CdS has a melting point of 1750 °C, precluding the molten phase filling of this material. Similarly, the formation of low-dimensional MS_2 (M=Mo,[22] W[23]) in multi-walled carbon nanotubes has been demonstrated by Wang *et al. via* the decomposition of molecular complexes demonstrating the further potential for tailoring bespoke semiconducting inorganic materials with nanoscale precision.

In this study, we evaluate carbon nanotubes as a nanoreactor in stepwise and one-pot inorganic syntheses, highlighting the advantages and limitations of the different approaches, and using the compounds of platinum as models, we outline a new strategy for the fabrication of inorganic nanomaterials with controlled structure and composition. Conducting the chemical transformations inside the host-nanotube allows structural determination of the reaction products with atomic precision by aberration corrected high resolution transmission electron microscopy (AC-HRTEM) and aberration corrected scanning transmission electron microscopy (AC-STEM), while our unique approach based on cross-correlation of fluorescence-detected X-ray absorption spectroscopy (FD-XAS) and Raman spectroscopy applied at each stage of inorganic synthesis in carbon nanotubes enables determination of the exact oxidation state of metal (Pt) in inorganic compounds formed inside nanotubes and the vibration characteristics of the host-nanotube respectively. This methodology enables changes in host-guest interactions from one stage of inorganic synthesis to another to be monitored by multiple techniques for the first time, providing a systematic understanding of the electron transfer between the nanoreactor and encapsulated compound during all stages of the formation process.

Results and Discussion:

The stepwise formation of inorganic materials in SWNTs is can be achieved by selecting an appropriate metal, i.e. small volatile metal complexes consisting of the required element for the desired inorganic material, and inserting them into the nanotube (figure 1a), followed by thermal treatment to release the metallic element into the nanotube cavity (figure 1b) with the sequential addition of a non-metallic element which reacts with the metal to form a desired inorganic compound. If necessary, more reaction steps can be added to convert the inorganic compound to another product (figure 1d).

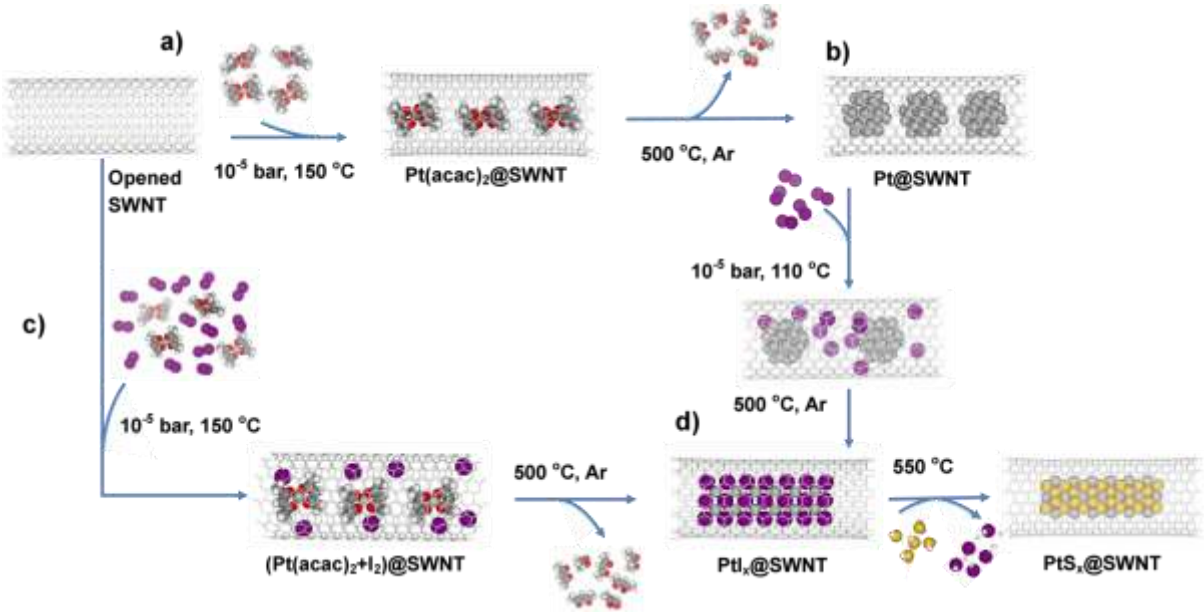

Figure 1: Schematic illustration depicting how inorganic materials can be formed using nanotubes as templates; a) the encapsulation of a selected metal precursor for the desired metallic element followed by thermal decomposition to form metal nanoparticles@SWNT; b) the addition of the second element by adding a second precursor followed by chemical reaction to form the inorganic material; c) the formation of inorganic materials using a one-step filling process in which both precursors, metallic and non-metallic, are added at the same time followed by chemical reaction; d) the transformation of one encapsulated inorganic material to another by treatment with a suitable reagent inside the nanotube.

To explore and evaluate this approach for inorganic synthesis in SWNTs, platinum acetylacetonate, $Pt(acac)_2$ was inserted into SWNTs from the gas phase, and excess $Pt(acac)_2$ was removed from the exterior of SWNTs by applying a selective CH_2Cl_2 washing technique,[24] leaving only $Pt(acac)_2$ molecules that are encapsulated within the nanotube $Pt(acac)_2$@SWNT. For noble metals such as Pt, the L_{III} edge FD-XAS is derived from the electronic transition from 2p3/2 to 5d states. The whiteline intensity directly reflects the degree of occupancy of the 5d states and, thus, is a good indicator of oxidation state variation.[25]

The FD-XAS of $Pt(acac)_2$@SWNT shows a slight increase in the Pt L_{III} edge energy relative to that of a $Pt(acac)_2$ control sample (see supporting information, table S.1) indicating a small reduction of electron density on the Pt centres inside the nanotubes; (figure 2a) however, Raman spectroscopy (figure 2b) shows no shift in the G-band of the SWNT suggesting little or no charge transfer between the guest and the nanotube upon encapsualtion.[26] Heating $Pt(acac)_2$@SWNT under argon at 500 °C for one hour resulted in the decomposition of $Pt(acac)_2$ and the release of metallic Pt into the SWNT cavities in the

form of elongated nanoparticles with an average length of 1.5 nm as confirmed by TEM imaging (figure 2c inset). The energy of the Pt L_{III} edge in Pt@SWNT is increased significantly relative to bulk metallic platinum which suggests the host SWNT depletes electron density around the metal. This correlates well with a small but measurable red-shift of the G band in the Raman spectrum of the host-nanotubes, confirming that some electron transfer takes place from Pt to SWNT in the Pt@SWNT material, leading to platinum in an oxidation state slightly above zero (table 1).

In the next step, Pt@SWNT was treated with iodine vapour (figure 1b) leading to direct synthesis of platinum iodide inside nanotubes, PtI_2@SWNT, from the constituent elements (figure 2 d, inset). Raman spectroscopy shows that the G-band of the host-nanotube in PtI_2@SWNT returns to a similar position to that of empty SWNTs, and FD-XAS shows that the energy of the Pt edge of PtI_2@SWNT is similar to that of known Pt^{II} complexes (table 1), with both methods agreeing that no electron transfer takes place between the nanotube and charge-neutral compound PtI_2, which contrasts with the observed Pt to SWNT electron transfer in Pt@SWNT as described above, or SWNT to iodine electron transfer described for I_2@SWNT in the literature.[26] Addition of H_2S to PtI_2@SWNT led to the transformation of platinum iodide to the platinum sulfide compound PtS_2@SWNT (figure 1d) which in similar fashion to the iodide exhibits no electron transfer with the nanotube as the Raman G-band position in PtS_2@SWNT coincides with that of empty SWNTs. This is in agreement with FD-XAS showing a Pt excitation edge energy similar to that of known Pt^{IV} complexes (table 1), thus confirming a charge-neutral PtS_2 material inside the nanotube. This series of chemical transformations inside carbon nanotubes clearly illustrates that stepwise inorganic synthesis involving transformations of a metal complex to metal nanoparticles, to metal iodide and to metal sulfide can be achieved in SWNTs with each stage verified by TEM, as well as FD-XAS and Raman spectroscopy revealing the nature of the interactions between the inorganic compounds and the host-nanotube.

Table 1: Shifts of the Pt L_{III} FD-XAS edge energy for the different platinum materials in SWNTs with resepect to (w.r.t.) their free state, and shifts in the G-band in the Raman spectra of nanotubes filled with different platinum materials w.r.t. that of empty SWNTs.

Material	**Shift of FD-XAS edge edge energy w.r.t free compound/eV**	**Shift of G-band w.r.t empty SWNT/cm^{-1}**	**Direction of electron transfer**
$Pt(acac)_2$@SWNT	+0.5	0	No transfer observed
Pt@SWNT	+1.0	-4	Pt → SWNT
$Pt(acac)_2I_2$@SWNT	-1.5	+6	Pt ← SWNT
PtI_2@SWNT	+0.3	0	No transfer observed

$Pt(acac)_2(SCN)_2$@SWNT	-0.6	-5.0	Pt → SWNT
PtS_2@SWNT	+0.4 (relative to another known Pt^{IV} compound)	0	No transfer observed

In a separate experiment, both $Pt(acac)_2$ and I_2 were encapsulated in SWNT simultaneously, from the gas phase followed by heat treatment of the encapsulated molecules ($Pt(acac)_2$ + I_2)@SWNT that triggers a chemical reaction between $Pt(acac)_2$ and I_2 to form PtI_2@SWNT in one step, which is analogous to a popular one-pot synthetic approach in preparative chemistry in the absence of SWNTS. Thus formed platinum iodide appears to be identical to the same compound formed in the stepwise process above, which clearly indicates advantages of the one-pot synthesis in nanotubes, allowing for the bypass of several stages of the stepwise approach, i.e. $Pt(acac)_2$ insertion and thermal decomposition, followed by I_2 insertion into SWNTs. While both of these approaches appear to be effective in controlling the dimensions of inorganic nanostructures being strictly controlled by the diameter of SWNTs, detailed analysis of the elemental composition of the inorganic products reveals a problem of stoichiometry control. Unlike organic molecular compounds, inorganic materials have a capacity for non-stoichiometric ratios of the constituent elements, which is evident from energy dispersive X-ray (EDX) analysis indicating that the materials synthesised inside nanotubes in both approaches have a non-stoichiometric ratio of metal and halogen/chalcogen. Specifically, the content of iodine in PtI_2@SWNT appears to be consistently higher that predicted for PtI_2 (figure 2d), and traces of iodine still remain present in the nanotubes even after conversion of PtI_2@SWNT to PtS_2@SWNT (figure 2e). This observation clearly highlights the challenge of controlling the correct proportions of reactants in nanotubes: I_2 is more volatile than $Pt(acac)_2$ and has a lower vapour pressure which means that it will always be loaded into the nanotube in excess of the Pt precursor, thus making the removal of extra iodine difficult, even after platinum iodide is transformed into platinum sulfide (figure 2e). As even a small deviation from the exact stoichiometric composition causes drastic effects in the physiochemical properties of inorganic materials, such as in the case of silicon doping with N or B, or diamond doping with N, or boron nitride doping with C, effective control of the ratios of the elements is of paramount importance in inorganic synthesis at the nanoscale.

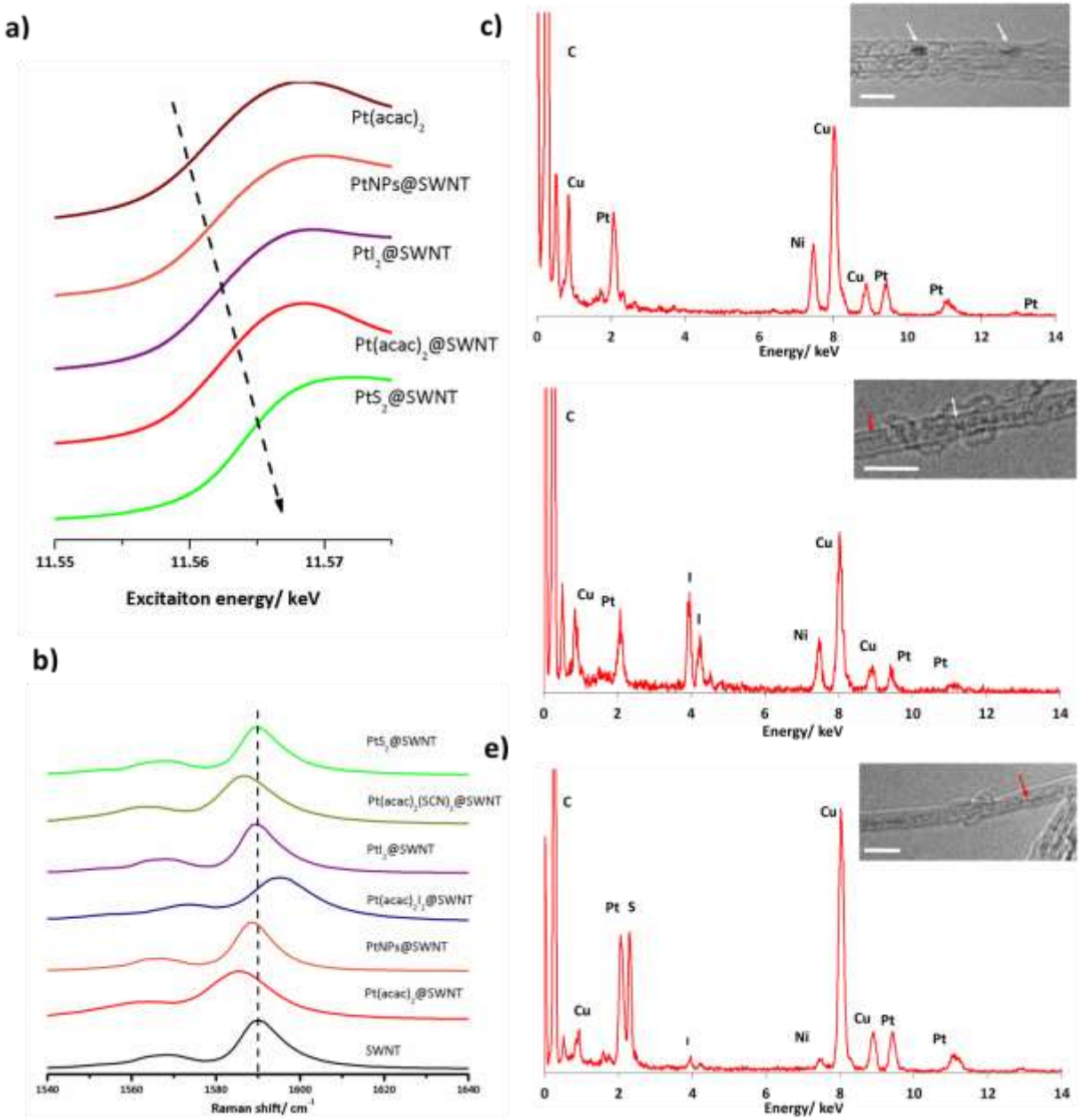

Figure 2: a) FD-XAS spectra showing the Pt L_{III} edge of materials in SWNTs using a stepwise approach compared to that of bulk $Pt(acac)_2$; b) Raman spectra showing how the G band of the nanotube shifts depending on the encapsulated material. The encapsulation of molecular species (Pt complexes or I_2) leads to electron transfers between the nanotube and guest; however, the encapsulated PtX (X = I or S) compounds exhibit no change in G-band meaning that no charge transfer is taking place. c) an EDX spectrum of Pt@SWNT, a low magnification TEM image (the white arrows showing Pt) of the sample is shown inset; d) an EDX spectrum of PtI_2@SWNT formed using the one-pot method. An excess of iodine is present in the sample. Inset is a TEM image showing clusters of Pt atoms (white arrow) and I atoms (red arrow) within the SWNT; and e) an EDX spectrum of PtS_2@SWNT formed from the treatment of PtI_2@SWNT with H_2S. Traces of iodine are still present in the sample. Inset is

a TEM image of PtS_2@SWNT formed by the transformation of PtI_2@SWNT. In agreement with the EDX spectrum, excess iodine is present (red arrow); (the scale bars are all 2nm, all EDX spectra were recorded at 100 keV primary electron energy and integrated over a small bundle of nanotubes. N.B. Cu peaks are due to the TEM specimen grid; Ni peaks are due to the catalyst used during SWNT formation).

A possible solution to this challenge can be found by designing a molecular precursor where the elements are present in the desired stoichiometric ratio for a specific inorganic product, which can then be encapsulated and converted into the inorganic material in SWNTs in a one-pot/one-reactant synthesis (figure 3). The advantage of such an approach is that it involves a single step and the stoichiometric ratio of the metal and halogen/chalcogen components in the material formed can be carefully tuned. The use of coordination compounds of transition metals offers excellent possibilities for controlling the composition and stoichiometry of the reactants. For example, the coordination environment of four-coordinate Pt complexes, such as $Pt(acac)_2$, can be expanded to six-coordinate by appending two extra ligands to the axial positions, which can carry the correct amounts of the desired non-metallic element (scheme 1). For example, the addition of two iodide or two thiocyanate ligands that occupy the two axial positions in the octahedral complex of Pt allows fixing of the ratio of metal to halogen or chalcogen to 1:2 thus ensuring the correct stoichiometry of the inorganic compound formed inside the nanotubes (figure 3).

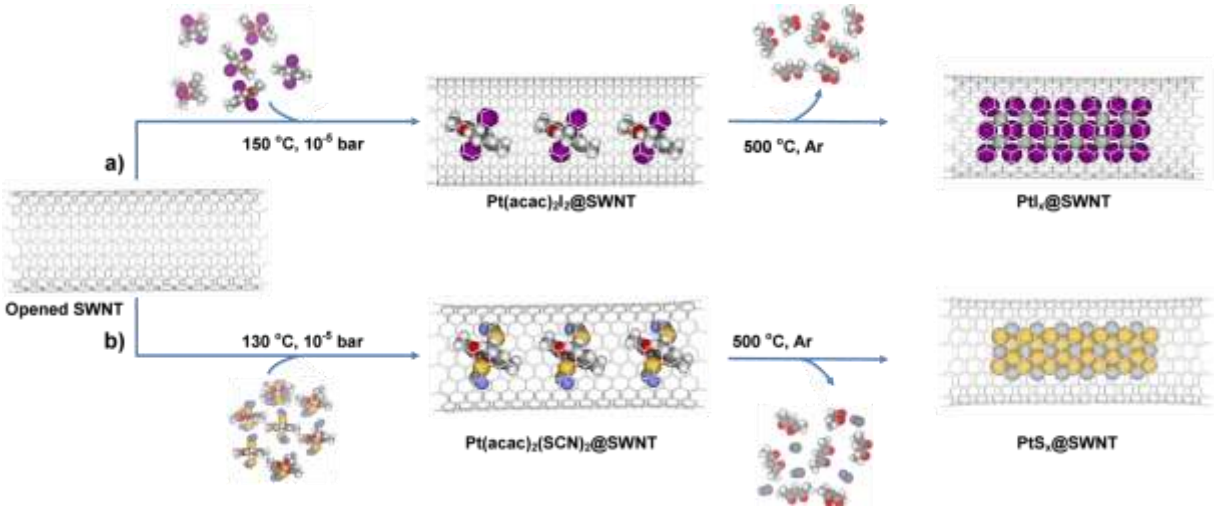

Figure 3: Schematic illustration depicting how inorganic materials can be formed using nanotubes as templates. The formation of a) PtI_2@SWNT; and b), PtS_2@SWNT are shown using our methodology. In general a molecular precursor which contains all of the required elements, in the correct stoichiometry for the desired inorganic material, is encapsulated. The thermal treatment of the

resultant precursor then leads to decomposition, chemical reaction to form the inorganic material in the nanotubes and expulsion of any volatile by-products into the gas phase.

To illustrate the principle of one-pot/one-reactant synthesis in nanoreactors, we prepared the molecular precursors *trans-bis*(acetylacetonato)di-iodoplatinum and *bis*(acetylacetonato)di-thiocyanatoplatinum containing Pt:I (1:2) and Pt:S (1:2) respectively by reacting $Pt(acac)_2$ with I_2 to give $Pt(acac)_2I_2$, and then reacting $Pt(acac)_2I_2$ with AgSCN to afford $Pt(acac)_2(SCN)_2$, using previously reported methods (scheme 1).[27, 28]

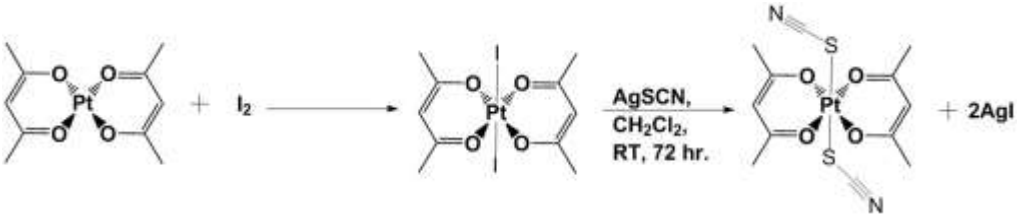

Scheme 1: The formation of $Pt(acac)_2I_2$ and $Pt(acac)_2(SCN)_2$ from $Pt(acac)_2$.

The resultant $Pt(acac)_2X_2$ (X = I, see figure 3a; SCN, see figure 3b) compounds were added to SWNTs and sealed in an ampoule under vacuum (10^{-5} bar). Heating at a temperature slightly above the sublimation points of the platinum complexes allowed the precursor molecules to penetrate the open ends of the nanotubes and become encapsulated. The excess material was removed from the nanotube surface by washing with CH_2Cl_2, leaving only molecules inserted in the nanotubes. Interestingly, the encapsulation of $Pt(acac)_2I_2$@SWNT led to a significant reduction in the absorption energy of the Pt L_{III} edge indicative of an increase of charge density onto the Pt centres as compared to free $Pt(acac)_2$ (figure 4a), which is complimented by a significant blue-shift of the Raman G-band of the host SWNT (figure 2b), implying electron transfer from the nanotube to the guest molecule which has not be observed for any other Pt compounds in this study. In contrast, $Pt(acac)_2(SCN)_2$@SWNT showed a decrease in the Pt edge energy in the FD-XAS (figure 4b) and a red-shift of the nanotube G band (figure 2b), indicating that the electron is transferred in the opposite direction to the previous complex, i.e. from SWNTs to $Pt(acac)_2(SCN)_2$. A simple thermal treatment led to the facile transformation of the molecular precursors to the desired inorganic structures, PtI_2@SWNT and PtS_2@SWNT (figure 3) with the stoichiometric 1:2 metal to halogen/chalcogen composition, as confirmed by EDX spectroscopy (figures 4c, d).

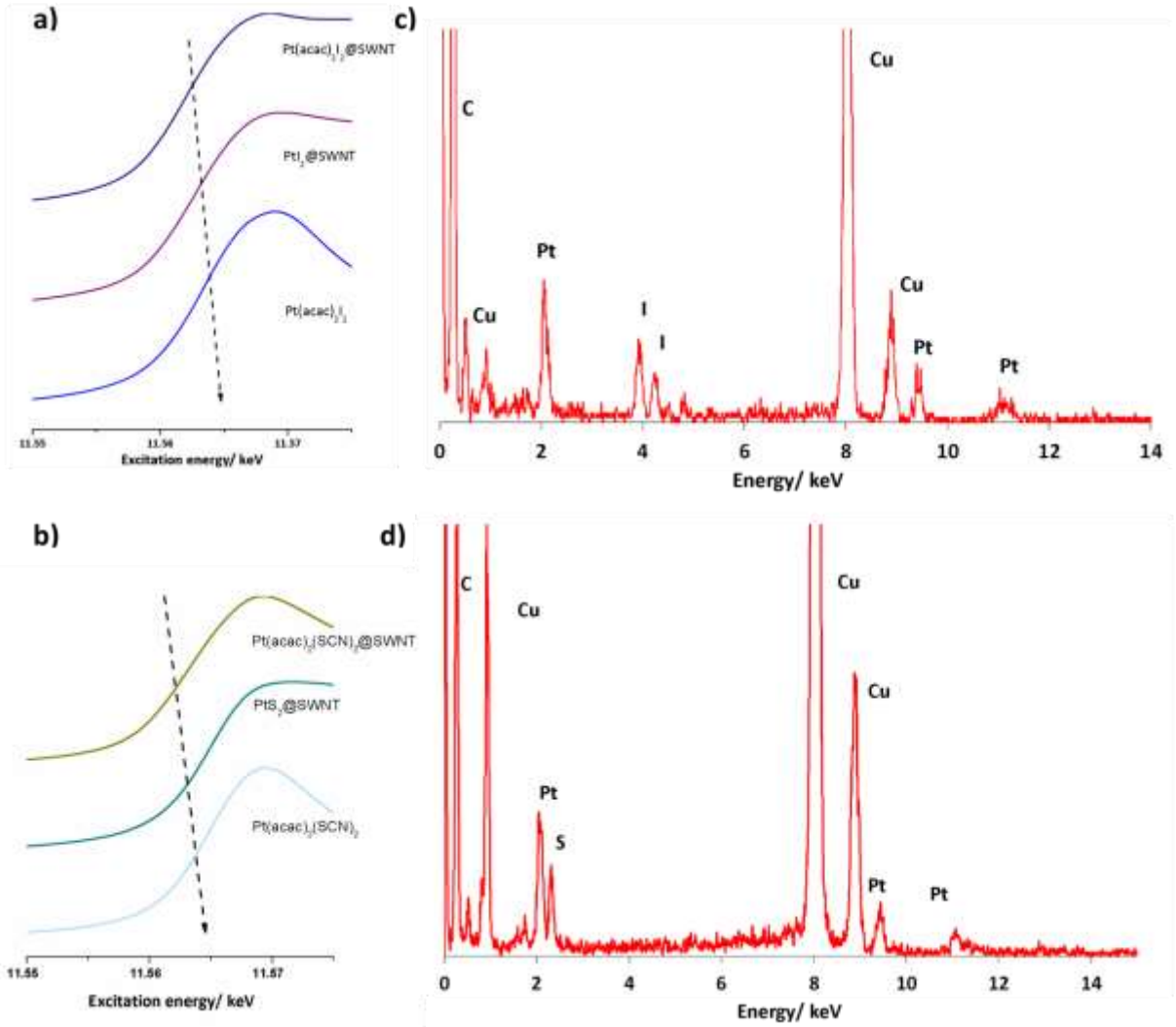

Figure 4: a and b) FD-XAS showing the Pt L_{III} edge of materials formed in SWNTs, using molecular precursors containing suitable amounts of material for the formation of PtI_2@SWNT (a) and PtS_2@SWNT (b); EDX spectra recorded at 100 keV primary electron energy and integrated over a small bundle of nanotubes showing c), PtI_2@SWNT; and d), PtS_2@SWNT, both formed *via* the thermal decomposition of molecular precursors containing the desired stoichiometric ratios of the two elements inside SWNTs. The spectra confirm the successful formation of the inorganic materials inside the nanotubes in each case (N.B. Cu peaks are due to the TEM specimen grid).

While the new one-pot/one-reactant approach clearly enabled a precise control of the stoichiometry, it is essential to verify the atomic structure of the inorganic compounds formed in this method, to ensure that the new molecular precursors still deliver inorganic materials with well-defined atomic structures. Aberration corrected high resolution TEM (AC-HRTEM) is the most direct tool for the structural characterisation of inorganic materials formed within SWNTs, as the precise atomic composition and any distortions in the crystal lattice can be clearly visualised to determine the effects

of nanoscale confinement.[23, 29, 30] TEM of the PtI_2@SWNT sample prepared by the one-pot/one-reactant approach revealed high filling of PtI_2 within the SWNTs (figure 5a) in which the entire channel was filled with the crystalline inorganic material. In a representative example, an individual filled nanotube with a diameter of ca. 1.52 nm, similar to that of an (11,11)SWNT (figure 5c), is observed to contain a quasi-one-dimensional PtI_2 crystal characterised by a close-packed cubic lattice (figure 5c) analogous to that of bulk PtI_2 (figure 5b) with only small lattice distortions observed in the confined nanocrystals compared to the bulk phase. Lattice measurements in experimental AC-HRTEM images showed regular spacings between atomic positions in the direction parallel to the nanotube of 0.388 nm, compared to a distance of 0.380 nm between I atoms in bulk PtI_2. Such a level of distortion in inorganic structures is consistent with the literature and is a result of the confined lattice adapting to the nanotube channel in order to increase van der Waals interactions with the nanotube sidewalls.[9, 17, 30] Similarly, there appears to be a slight increase in the diameter of the SWNT due to an elliptic distortion of the nanotube channel to accommodate the PtI_2 species (figure 5d and e) which has also been reported previously for such systems.[19] Computational modelling was utilised to generate a 3D model of PtI_2@SWNT to enable comparison with experimental AC-HRTEM images. Scherzer defocussed AC-HRTEM images were then calculated for a (11,11)SWNT and the derived crystal fragment using QSTEM TEM simulation and are in good agreement with the experimentally obtained images (figure 5c, d, and e).

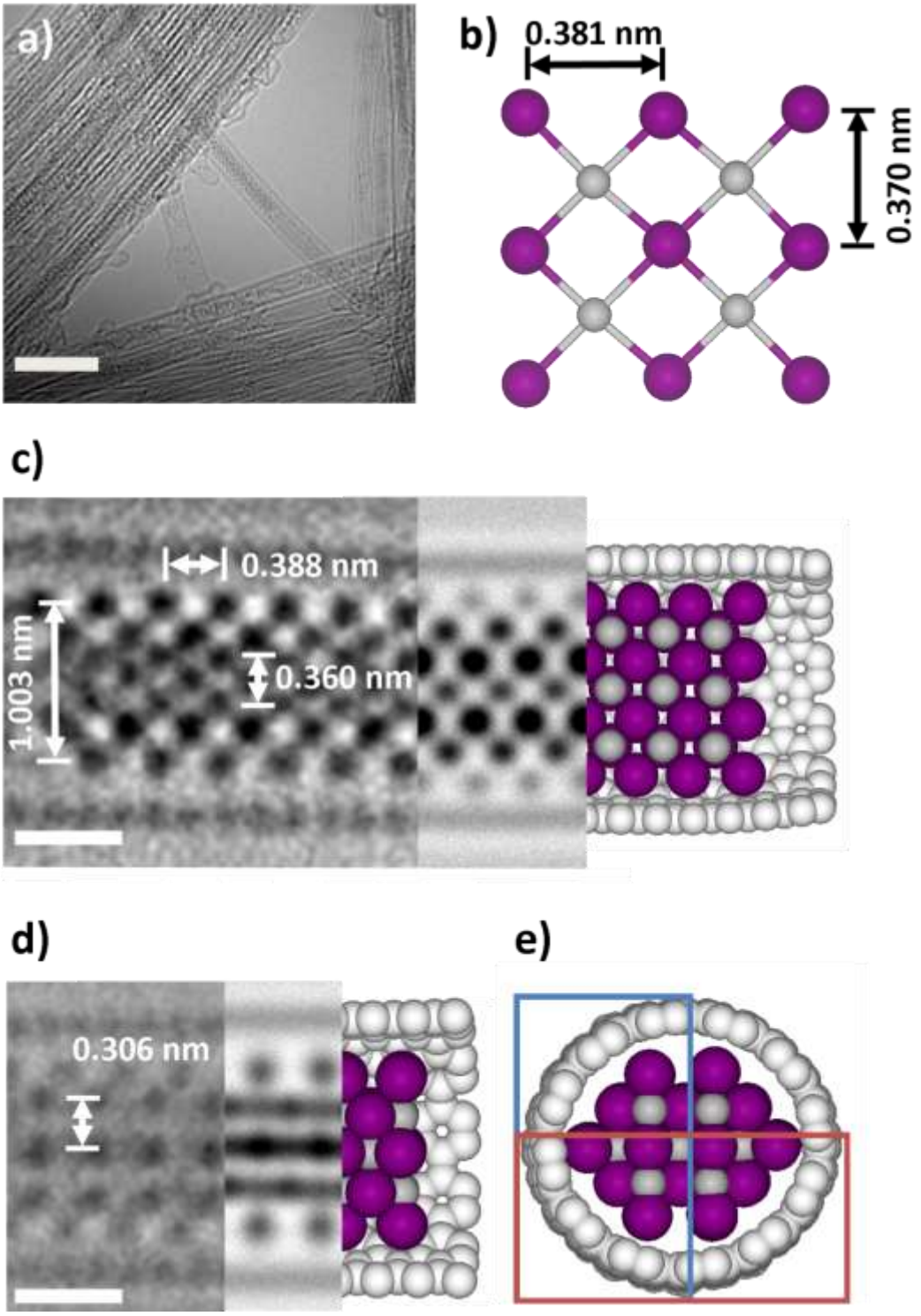

Figure 5: a) An AC-HRTEM micrograph showing a bundle of PtI_2@SWNT in which the majority of the SWNTs are highly filled with inorganic material, the scale bar is 5 nm; b) An extended portion of the crystal structure of bulk PtI_2 with key atomic distances shown; the grey and purple spheres represent platinum and iodine atoms respectively; c) an AC-HRTEM micrograph showing a small section of a 1.52 nm SWNT containing PtI_2 material and the corresponding atomic distances to the bulk structure in b) are shown. A QSTEM simulation (80 kV) showing a projection of how a portion of the bulk PtI_2

structure could fit inside an (11,11) SWNT, complimented by the cross-section of computational simulation to show its shape in the nanotube, the scale bar is 0.5 nm; d) an AC-HRTEM of the same section of nanotube with the material in a different orientation is shown, along with a QSTEM simulation (80 kV) showing a projection of the model from (c) when rotated 90° parallel to the nanotube axis, and a computational simulation of this model to show its shape in the nanotube, the scale bar is 5 nm; and e) a simulation to show how the crystal fragment would appear when looking down the nanotube. The red and blue boxes represent the sections of the tube visible in figures c and d respectively.

In bright-field AC-HRTEM images (figure 5) the observed contrast of atoms is proportional to $Z^{0.5}$, where Z is the atomic number of the element which usually results in large differences in contrast between heavy and light elements making it easy to discriminate between them, however this technique is less efficient at distinguishing between two heavy elements such as Pt and I present in our material. Consequently, it is important to confirm the identities of the atoms within the lattice using a complimentary technique, aberration-corrected scanning transmission electron microscopy (AC-STEM). With AC-STEM the intensity of contrast is proportional to Z^{α}, where α depends on the detector angle and is typically 1.7-1.8[31] making it easier to distinguish between two heavy atoms within the same structure. AC-STEM images of PtI_2@SWNT clearly show a cubic lattice (figure 6a), similar to that observed with AC-HRTEM and correlates well with the bulk crystal structure of PtI_2.

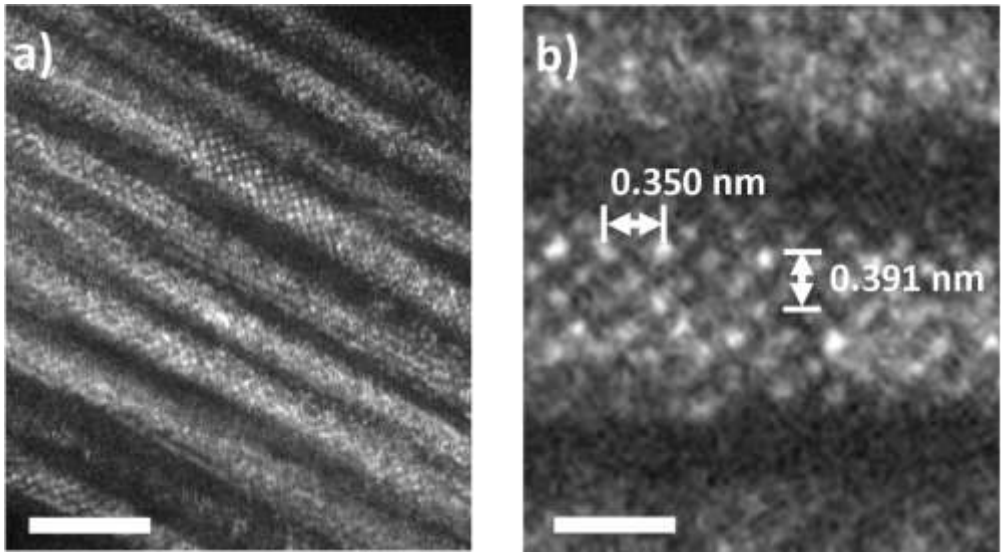

Figure 6 a) AC-STEM image showing a bundle of PtI_2@SWNT in which the majority of the SWNTs are highly filled with inorganic material, the scale bar is 3 nm; b) AC-STEM showing micrograph showing a small section of a SWNT containing PtI_2 material and the corresponding atomic distances to the

bulk structure, the material adopts a cubic configuration analogous to that observed in the bright field images in figure 5.

AC-HRTEM images of PtS_2@SWNT material prepared in the one-pot/one-reactant synthesis clearly show extended inorganic nanostructures within the channels of SWNTs (figure 7a). In contrast to the encapsulated PtI_2@SWNT, only platinum atoms can be visualised by AC-HRTEM in this sample due to the significant difference between the atomic numbers of sulfur and platinum. The encapsulated material in PtS_2@SWNT is characterised by a hexagonal lattice analogous to that of bulk PtS_2 (figure 7b). The edge of the encapsulated PtS_2 adopts a zigzag conformation, with only sulfur atoms in contact with the nanotube sidewall. Whilst there is a negligible decrease in the Pt-Pt separations of the encapsulated PtS_2 in the direction parallel to the nanotube compared to the bulk PtS_2, there is a larger decrease in the orthogonal direction. This assignment is in agreement with the Scherzer defocussed AC-HRTEM image calculated for a crystal fragment of PtS_2 inside (11,11)SWNT which exhibits structural features consistent with the experimentally obtained AC-HRTEM images (figure 7c).

An AC-STEM image of PtS_2@SWNT (figure 7d) clearly shows a hexagonal lattice of Pt atoms matching that in AC-HRTEM images for this material (figure 7c). The Pt-Pt spacings appear to be in much closer agreement with bulk PtS_2 with only a small increase in the direction parallel to the principal SWNT axis. Although the nanotube sidewall cannot be observed in AC-STEM, in contrast to the images obtained using bright field TEM, only three layers of platinum atoms are present in this sample suggesting that the host nanotube is narrower.

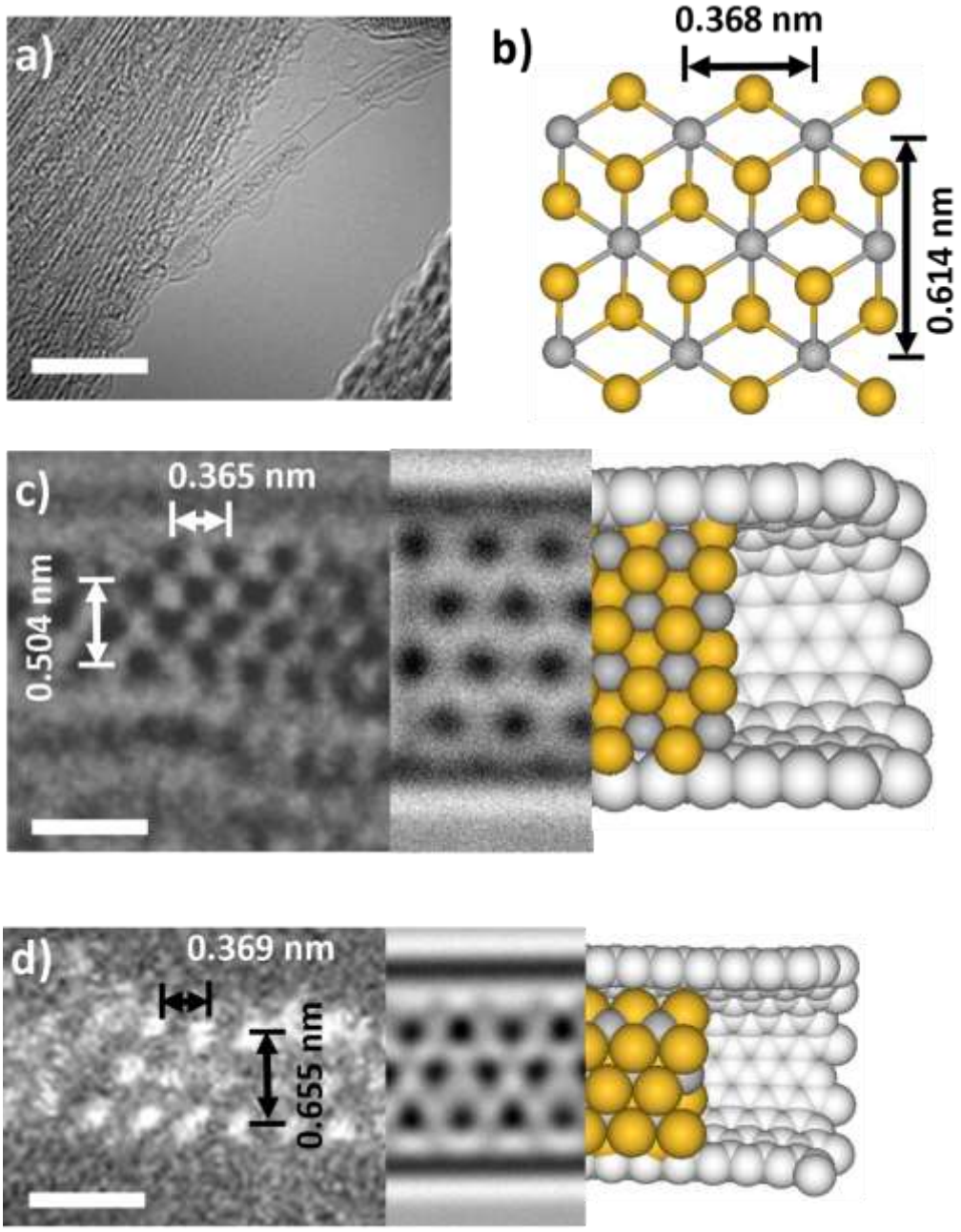

Figure 7: a) An AC-HRTEM micrograph showing a bundle of nanotubes containing PtS_2 material. The majority of SWNTs appear to be highly filled, and a single standing tube is visible, the scale bar is 5 nm; b) a portion of the crystal structure of bulk PtS_2, with key atomic distances shown; the grey and yellow spheres represent platinum and sulfur atoms respectively; c) an AC-HRTEM micrograph showing a small section of a 1.32 nm SWNT containing PtS_2 and interatomic distances corresponding to the distances in 7b are shown; a QSTEM simulation (80 kV) showing how PtS_2 could fit inside a SWNT, complimented by a computational simulation to show its morphology in the nanotube; d) an AC-STEM image showing what appears to be a single strand of PtS_2 in a SWNT, the material adopts a

hexagonal configuration analogous to that shown in c); however, there are only three layers of atoms present suggesting that the nanotube is narrower; furthermore, a QSTEM simulation (80 kV) showing how PtS_2 could fit inside a (11,11) SWNT, complimented by a simulation to show its morphology in the nanotube.

Conclusions

Inorganic synthesis at the nanoscale is an important, but challenging task because of the need for simultaneous control of the dimensionality and stoichiometry of nanostructures. Carbon nanotubes, acting as nanocontainers effectively provide strict control of the size and shape of nanostructures, as we have demonstrated in this study by employing SWNTs as reaction vessels for the direct inorganic synthesis of a series of Pt compounds at the nanoscale. A detailed comparison of the stepwise and one-pot synthetic approaches clearly illustrates the advantages of the latter in terms of efficiency. However, the stepwise approach offers an excellent opportunity for studying the mechanisms of host-guest interactions between the SWNT and encapsulated compounds. We have shown that a combination of FD-XAS and Raman spectroscopy can probe both the inorganic compound and the nanotube properties, and shed light on the direction and magnitude of electron transfer between the nanotube and compound inside. For example, two structurally related Pt complexes $Pt(acac)_2I_2$ and $Pt(acac)_2(SCN)_2$ have shown opposing electronic interactions with SWNTs, withdrawing or donating electron density from/to the host-nanotube, which alters both the oxidation state of the Pt and the vibrational properties of the SWNT. However, neither one-pot nor stepwise approaches appeared to be able to provide sufficient control of the stoichiometry in the inorganic products formed inside the nanotube.

We found a solution to this problem by exploiting the diversity of the coordination chemistry of Pt complexes acting as precursors for the inorganic nanostructures. We expanded the coordination environment of the Pt-atom in the precursor complex by appending extra ligands bearing the necessary elements (I or S) in a correct and precise proportion to Pt, thus paving the way to stoichiometrically controlled synthesis inside nanotubes, as demonstrated by the synthesis of novel PtI_2@SWNT and PtS_2@SWNT nanostructures in the new one-pot/one-reactant approach with the specifically designed multi-element containing precursors. The new strategy for inorganic synthesis at the nanoscale was shown to be versatile and universal, enabling the formation of previously inaccessible quasi-one-dimensional Pt-containing nanomaterials suitable for a variety of technological applications. These range from electronic devices where electronic doping of the nanotube is precisely modulated by electron transfer between the SWNT and encapsulated compound, to new catalytic platforms

exploiting the unique chemical properties of platinum compounds, where the shape of the crystal and oxidation state of the metal are controlled by steric and electron interactions with the host-nanotube.

Experimental

Materials

SWNTs (P2-SWNTs, arc discharge, Carbon Solutions, USA) were annealed at 600 °C for 15 min to open their termini and remove any residual amorphous carbon from their internal cavities resulting in a 50% weight loss being observed. The platinum precursor, $Pt(acac)_2$ was used as supplied (Sigma Aldrich). The substituted platinum precursors $Pt(acac)_2I_2$[27] and $Pt(acac)_2(SCN)_2$[28] were synthesised in accordance with published procedures.

PtI_2@SWNT

$Pt(acac)_2$ (90 mg, 0.229 mmol) and freshly opened SWNTs (25 mg) were sealed together under vacuum (10^{-6} bar) in a Pyrex ampoule and heated at 150 °C for 3 days to ensure penetration of the SWNT by the $Pt(acac)_2$. The sample was cooled rapidly and repetitive washing with dichloromethane (4 x 25 mL) was performed to remove any excess material from the exterior of the SWNTs, forming $Pt(acac)_2$@SWNT. Under at atmosphere of argon, $Pt(acac)_2$@SWNT (10 mg, 0.0196 mmol) was heated at 500 °C for 1 h and allowed to cool down slowly forming Pt@SWNT. This sample was sealed in a Pyrex ampoule with an excess of I_2 and heated at 110 °C for 3 days to give PtI_2@SWNT.

Alternatively, $Pt(acac)_2I_2$ (10 mg 0.0192 mmol) was sealed under vacuum with SWNTs (5 mg) and heated for 3 days at 150 °C. The sample was cooled rapidly and heated under argon at 500 °C for 1 h to give PtI_2@SWNT

PtS_2@SWNT

Argon was passed over PtI_2@SWNT (5.7 mg) for 1 h. The sample was then heated in the presence of H_2S (10 bar) at 550 °C for 2 h. The sample was then allowed to cool by 5 °C/min under argon.

Alternatively, $Pt(acac)_2(SCN)_2$ (10 mg, 0.0196 mmol) was sealed under vacuum with SWNTs (5 mg) and heated at 130 °C for 3 days. After washing with chloroform (4 x 10 mL), the sample was heated under argon at 500 °C for 1 h to give PtS_2@SWNT.

Electron Microscopy

SWNTs filled with the encapsulated materials were dispersed in propan-2-ol using an ultrasonic bath and drop cast onto lacey carbon-coated copper TEM grids (Agar). HRTEM imaging and electron beam

irradiation was carried out on a JEOL 2100 FEG-TEM microscope operated at 200 kV. Aberration-corrected TEM was performed at the University of Ulm on a C_s corrected FEI Titan 80-300 TEM operated at 80 kV with information limit enhancement using reduced extraction voltage. AC-STEM was performed at the University of Birmingham using a 200 kV JEOL 2100F microscope fitted with a high angle annular dark field (HAADF) detector.

EDX Spectroscopy

Local EDX spectra were acquired for samples mounted on TEM grids using an Oxford Instruments INCA X-ray microanalysis system. The electron beam was condensed onto areas of specimens (bulk specimen or nanotube bundles) suspended over holes of the amorphous carbon film.

Raman Spectroscopy

The samples were separately dispersed in propan-2-ol, mounted onto Si(100) supports, and their Raman spectra were recorded at room temperature (HoribaJY LabRAM HR spectro-meter, laser wavelength 532 nm).

Image Simulation

TEM image simulation was carried out using the multislice program QSTEM. QSTEM uses the Dirac-Fock scattering potential of Rez *et al*.[32] A fixed number of 20 slices per nanotube was chosen and images were calculated with a sampling of 0.05 nm per pixel. The aberration coefficients and defocus parameters *df, C*S, *A1*, and *B*2 were set according to the imaging conditions in the specific experiment. The convergence angle was fixed at 0.5 mrad. The effect of limited electron dose was emulated by applying noise to the calculated images using a custom-made Monte-Carlo program exploiting the Poisson statistics of electrons. Atomic models of SWNTs were built using a custom-made program taking into account different nanotube chiralities, if determinable in the experimental images. The structural models of the inorganic nanomaterials are based on scaled bulk structures and the complex models (PtX@SWNT) are rendered and iteratively fitted to the experimental results.

Fluorescence-Detected X-ray Absorption Spectroscopy (FD-XAS)

All FD-XAS measurements were carried out on the XMaS beamline (BM28) at the ESRF. Samples were deposited onto carbon tape, which was then mounted onto a stainless steel sample holder. FD-XAS edge inflection points were obtained by fitting a smoothing spline to the measured spectrum, and taking the first derivative of the fitted spectrum.

References

1. Govindaraj, A.; Satishkumar, B. C.; Nath, M.; Rao, C. N. R., Metal nanowires and intercalated metal layers in single-walled carbon nanotube bundles. *Chem. Mater.* **2000,** *12* (1), 202-205.
2. Kiang, C. H.; Choi, J. S.; Tran, T. T.; Bacher, A. D., Molecular nanowires of 1 nm diameter from capillary filling of single-walled carbon nanotubes. *J. Phys. Chem. B* **1999,** *103* (35), 7449-7451.
3. Nakanishi, R.; Kitaura, R.; Ayala, P.; Shiozawa, H.; de Blauwe, K.; Hoffmann, P.; Choi, D.; Miyata, Y.; Pichler, T.; Shinohara, H., Electronic structure of Eu atomic wires encapsulated inside single-wall carbon nanotubes. *Physical Review B* **2012,** *86* (11).
4. Yanagi, K.; Miyata, Y.; Kataura, H., Highly stabilized beta-carotene in carbon nanotubes. *Adv. Mater.* **2006,** *18* (4), 437-+.
5. Takenobu, T.; Takano, T.; Shiraishi, M.; Murakami, Y.; Ata, M.; Kataura, H.; Achiba, Y.; Iwasa, Y., Stable and controlled amphoteric doping by encapsulation of organic molecules inside carbon nanotubes. *Nature Materials* **2003,** *2* (10), 683-688.
6. Ren, Y.; Pastorin, G., Incorporation of hexamethylmelamine inside capped carbon nanotubes. *Adv. Mater.* **2008,** *20* (11), 2031-+.
7. Kiselev, N. A.; Kumskov, A. S.; Zhigalina, V. G.; Verbitskiy, N. I.; Yashina, L. V.; Chuvilin, A. L.; Vasiliev, A. L.; Eliseev, A. A.; Iop, The structure and electronic properties of copper iodide 1D nanocrystals within single walled carbon nanotubes. In *18th Microscopy of Semiconducting Materials Conference*, Walther, T.; Hutchison, J. L., Eds. 2013; Vol. 471.
8. Meyer, R. R.; Sloan, J.; Dunin-Borkowski, R. E.; Kirkland, A. I.; Novotny, M. C.; Bailey, S. R.; Hutchison, J. L.; Green, M. L. H., Discrete atom imaging of one-dimensional crystals formed within single-walled carbon nanotubes. *Science* **2000,** *289* (5483), 1324-1326.
9. Sloan, J.; Grosvenor, S. J.; Friedrichs, S.; Kirkland, A. I.; Hutchison, J. L.; Green, M. L. H., A one-dimensional BaI2 chain with five- and six-coordination, formed within a single-walled carbon nanotube. *Angewandte Chemie-International Edition* **2002,** *41* (7), 1156-+.
10. Hulman, M.; Costa, P.; Green, M. L. H.; Friedrichs, S.; Kuzmany, H., Raman spectroscopy of PbO-filled single wall carbon nanotubes. In *Electronic Properties of Synthetic Nanostructures*, Kuzmany, H.; Fink, J.; Mehring, M.; Roth, S., Eds. Amer Inst Physics: Melville, 2004; Vol. 723, pp 278-281.
11. Flahaut, E.; Sloan, J.; Friedrichs, S.; Kirkland, A. I.; Coleman, K. S.; Williams, V. C.; Hanson, N.; Hutchison, J. L.; Green, M. L. H., Crystallization of 2H and 4H PbI2 in carbon nanotubes of varying diameters and morphologies. *Chem. Mater.* **2006,** *18* (8), 2059-2069.
12. Satishkumar, B. C.; Taubert, A.; Luzzi, D. E., Filling single-wall carbon nanotubes with d- and f-metal chloride and metal nanowires. *Journal of Nanoscience and Nanotechnology* **2003,** *3* (1-2), 159-163.
13. Chuvilin, A.; Bichoutskaia, E.; Gimenez-Lopez, M. C.; Chamberlain, T. W.; Rance, G. A.; Kuganathan, N.; Biskupek, J.; Kaiser, U.; Khlobystov, A. N., Self-assembly of a sulphur-terminated graphene nanoribbon within a single-walled carbon nanotube. *Nature Materials* **2011,** *10* (9), 687-692.
14. Chamberlain, T. W.; Biskupek, J.; Rance, G. A.; Chuvilin, A.; Alexander, T. J.; Bichoutskaia, E.; Kaiser, U.; Khlobystov, A. N., Size, Structure, and Helical Twist of Graphene Nanoribbons Controlled by Confinement in Carbon Nanotubes. *Acs Nano* **2012,** *6* (5), 3943-3953.
15. Shi, L.; Rohringer, P.; Suenaga, K.; Niimi, Y.; Kotakoski, J.; Meyer, J. C.; Peterlik, H.; Wanko, M.; Cahangirov, S.; Rubio, A.; Lapin, Z. J.; Novotny, L.; Ayala, P.; Pichler, T., Confined linear carbon chains as a route to bulk carbyne. *Nat Mater* **2016,** *advance online publication*.
16. Geim, A. K.; Grigorieva, I. V., Van der Waals heterostructures. *Nature* **2013,** *499* (7459), 419-425.
17. Xu, C. G.; Sloan, J.; Brown, G.; Bailey, S.; Williams, V. C.; Friedrichs, S.; Coleman, K. S.; Flahaut, E.; Hutchison, J. L.; Dunin-Borkowski, R. E.; Green, M. L. H., 1D lanthanide halide crystals inserted into single-walled carbon nanotubes. *Chem. Commun.* **2000,** (24), 2427-2428.

18. Sloan, J.; Novotny, M. C.; Bailey, S. R.; Brown, G.; Xu, C.; Williams, V. C.; Friedrichs, S.; Flahaut, E.; Callender, R. L.; York, A. P. E.; Coleman, K. S.; Green, M. L. H.; Dunin-Borkowski, R. E.; Hutchison, J. L., Two layer 4 : 4 co-ordinated KI crystals grown within single walled carbon nanotubes. *Chem. Phys. Lett.* **2000,** *329* (1-2), 61-65.
19. Philp, E.; Sloan, J.; Kirkland, A. I.; Meyer, R. R.; Friedrichs, S.; Hutchison, J. L.; Green, M. L. H., An encapsulated helical one-dimensional cobalt iodide nanostructure. *Nature Materials* **2003,** *2* (12), 788-791.
20. Yashina, L. V.; Eliseev, A. A.; Kharlamova, M. V.; Volykhov, A. A.; Egorov, A. V.; Savilov, S. V.; Lukashin, A. V.; Puttner, R.; Belogorokhov, A. I., Growth and Characterization of One-Dimensional SnTe Crystals within the Single-Walled Carbon Nanotube Channels. *J. Phys. Chem. C* **2011,** *115* (9), 3578-3586.
21. Eliseev, A. A.; Chernysheva, M. V.; Verbitskii, N. I.; Kiseleva, E. A.; Lukashin, A. V.; Tretyakov, Y. D.; Kiselev, N. A.; Zhigalina, O. M.; Zakalyukin, R. M.; Vasiliev, A. L.; Krestinin, A. V.; Hutchison, J. L.; Freitag, B., Chemical Reactions within Single-Walled Carbon Nanotube Channels. *Chem. Mater.* **2009,** *21* (21), 5001-5003.
22. Wang, Z.; Li, H.; Liu, Z.; Shi, Z.; Lu, J.; Suenaga, K.; Joung, S.-K.; Okazaki, T.; Gu, Z.; Zhou, J.; Gao, Z.; Li, G.; Sanvito, S.; Wang, E.; Iijima, S., Mixed Low-Dimensional Nanomaterial: 2D Ultranarrow MoS2 Inorganic Nanoribbons Encapsulated in Quasi-1D Carbon Nanotubes. *J. Am. Chem. Soc.* **2010,** *132* (39), 13840-13847.
23. Wang, Z.; Zhao, K.; Li, H.; Liu, Z.; Shi, Z.; Lu, J.; Suenaga, K.; Joung, S.-K.; Okazaki, T.; Jin, Z.; Gu, Z.; Gao, Z.; Iijima, S., Ultra-narrow WS2 nanoribbons encapsulated in carbon nanotubes. *J. Mater. Chem.* **2011,** *21* (1), 171-180.
24. Fu, Q.; Weinberg, G.; Su, D.-s., Selective filling of carbon nanotubes with metals by selective washing. *New Carbon Materials* **2008,** *23* (1), 17-20.
25. Zhang, F.; Jiao, F.; Pan, X. L.; Gao, K.; Xiao, J. P.; Zhang, S.; Bao, X. H., Tailoring the Oxidation Activity of Pt Nanoclusters via Encapsulation. *Acs Catalysis* **2015,** *5* (2), 1381-1385.
26. Grigorian, L.; Williams, K. A.; Fang, S.; Sumanasekera, G. U.; Loper, A. L.; Dickey, E. C.; Pennycook, S. J.; Eklund, P. C., Reversible intercalation of charged iodine chains into carbon nanotube ropes. *Phys. Rev. Lett.* **1998,** *80* (25), 5560-5563.
27. Cook, P. M.; Dahl, L. F.; Hopgood, D.; Jenkins, R. A., OXIDATIVE-ADDITION REACTION OF PLATINUM ACETYLACETONATE WITH IODINE IN SOLID-STATE AND SOLUTION - CRYSTAL-STRUCTURE AND EQUILIBRIUM STUDIES OF TRANS-BIS(ACETYLACETONATO)DI-IODOPLATINUM(IV). *Journal of the Chemical Society-Dalton Transactions* **1973,** (3), 294-301.
28. Grabowski, A.; Preetz, W., PREPARATION AND VIBRATIONAL-SPECTRA OF TRANS-PT(ACAC)2CL2 , TRANS- PT(ACAC)2BR2 , TRANS- PT(ACAC)2I2 , TRANS- PT(ACAC)2SCN2 , TRANS-PT(ACAC)2SECN2 , TRANS- PT(ACAC)2N-3(2). *Z. Anorg. Allg. Chem.* **1987,** *544* (1), 95-100.
29. Eliseev, A. A.; Yashina, L. V.; Verbitskiy, N. I.; Brzhezinskaya, M. M.; Kharlamova, M. V.; Chernysheva, M. V.; Lukashin, A. V.; Kiselev, N. A.; Kumskov, A. S.; Freitag, B.; Generalov, A. V.; Vinogradov, A. S.; Zubavichus, Y. V.; Kleimenov, E.; Nachtegaal, M., Interaction between single walled carbon nanotube and 1D crystal in CuX@SWCNT (X = Cl, Br, I) nanostructures. *Carbon* **2012,** *50* (11), 4021-4039.
30. Kiselev, N. A.; Zakalyukin, R. M.; Zhigalina, O. M.; Grobert, N.; Kumskov, A. S.; Grigoriev, Y. V.; Chernysheva, M. V.; Eliseev, A. A.; Krestinin, A. V.; Tretyakov, Y. D.; Freitag, B.; Hutchison, J. L., The structure of 1D CuI crystals inside SWNTs. *Journal of Microscopy* **2008,** *232* (2), 335-342.
31. Wang, Z. W.; Li, Z. Y.; Park, S. J.; Abdela, A.; Tang, D.; Palmer, R. E., Quantitative Z-contrast imaging in the scanning transmission electron microscope with size-selected clusters. *Physical Review B* **2011,** *84* (7).
32. Rez, D.; Rez, P.; Grant, I., DIRAC-FOCK CALCULATIONS OF X-RAY-SCATTERING FACTORS AND CONTRIBUTIONS TO THE MEAN INNER POTENTIAL FOR ELECTRON-SCATTERING. *Acta Crystallographica Section A* **1994,** *50*, 481-497.